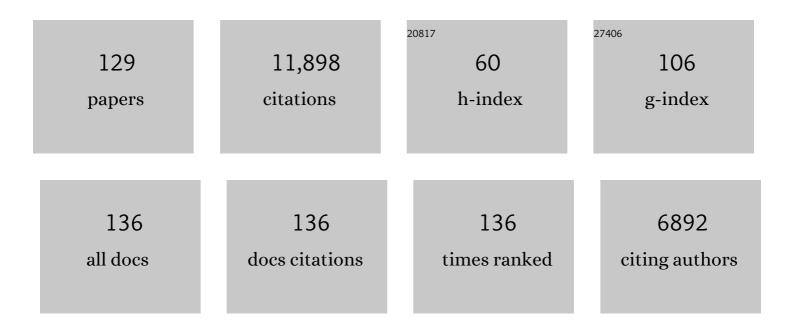
Mark Simons

List of Publications by Year in descending order

Source: https://exaly.com/author-pdf/7857111/publications.pdf Version: 2024-02-01



#	Article	IF	CITATIONS
1	The 2011 Magnitude 9.0 Tohoku-Oki Earthquake: Mosaicking the Megathrust from Seconds to Centuries. Science, 2011, 332, 1421-1425.	12.6	648
2	Updated repeat orbit interferometry package released. Eos, 2004, 85, 47-47.	0.1	505
3	The complete (3-D) surface displacement field in the epicentral area of the 1999MW7.1 Hector Mine Earthquake, California, from space geodetic observations. Geophysical Research Letters, 2001, 28, 3063-3066.	4.0	458
4	Frictional Afterslip Following the 2005 Nias-Simeulue Earthquake, Sumatra. Science, 2006, 312, 1921-1926.	12.6	440
5	Three-dimensional deformation caused by the Bam, Iran, earthquake and the origin of shallow slip deficit. Nature, 2005, 435, 295-299.	27.8	403
6	Coseismic Deformation from the 1999 Mw 7.1 Hector Mine, California, Earthquake as Inferred from InSAR and GPS Observations. Bulletin of the Seismological Society of America, 2002, 92, 1390-1402.	2.3	384
7	Some thoughts on the use of InSAR data to constrain models of surface deformation: Noise structure and data downsampling. Geochemistry, Geophysics, Geosystems, 2005, 6, n/a-n/a.	2.5	332
8	Deformation and Slip Along the Sunda Megathrust in the Great 2005 Nias-Simeulue Earthquake. Science, 2006, 311, 1897-1901.	12.6	284
9	Hierarchical interlocked orthogonal faulting in the 2019 Ridgecrest earthquake sequence. Science, 2019, 366, 346-351.	12.6	284
10	Deformation due to a pressurized horizontal circular crack in an elastic half-space, with applications to volcano geodesy. Geophysical Journal International, 2001, 146, 181-190.	2.4	272
11	A satellite geodetic survey of large-scale deformation of volcanic centres in the central Andes. Nature, 2002, 418, 167-171.	27.8	250
12	Large Trench-Parallel Gravity Variations Predict Seismogenic Behavior in Subduction Zones. Science, 2003, 301, 630-633.	12.6	247
13	Localized gravity/topography admittance and correlation spectra on Mars: Implications for regional and global evolution. Journal of Geophysical Research, 2002, 107, 19-1-19-25.	3.3	243
14	Superficial simplicity of the 2010 El Mayor–Cucapah earthquake of Baja California in Mexico. Nature Geoscience, 2011, 4, 615-618.	12.9	225
15	Improving InSAR geodesy using Global Atmospheric Models. Journal of Geophysical Research: Solid Earth, 2014, 119, 2324-2341.	3.4	220
16	Bayesian inversion for finite fault earthquake source models l—theory and algorithm. Geophysical Journal International, 2013, 194, 1701-1726.	2.4	206
17	Localization of gravity and topography: constraints on the tectonics and mantle dynamics of Venus. Geophysical Journal International, 1997, 131, 24-44.	2.4	192
18	Deformation on Nearby Faults Induced by the 1999 Hector Mine Earthquake. Science, 2002, 297, 1858-1862.	12.6	171

#	Article	IF	CITATIONS
19	An InSAR-based survey of volcanic deformation in the central Andes. Geochemistry, Geophysics, Geosystems, 2004, 5, n/a-n/a.	2.5	167
20	Neutral atmospheric delay in interferometric synthetic aperture radar applications: Statistical description and mitigation. Journal of Geophysical Research, 2003, 108, .	3.3	163
21	Complex rupture during the 12 January 2010 HaitiÂearthquake. Nature Geoscience, 2010, 3, 800-805.	12.9	157
22	Correction to "Localized gravity/topography admittance and correlation spectra on Mars: Implications for regional and global evolutionâ€: Journal of Geophysical Research, 2004, 109, .	3.3	151
23	A Network-Based Enhanced Spectral Diversity Approach for TOPS Time-Series Analysis. IEEE Transactions on Geoscience and Remote Sensing, 2017, 55, 777-786.	6.3	141
24	Multiscale dynamics of the Tonga-Kermadec subduction zone. Geophysical Journal International, 2003, 153, 359-388.	2.4	139
25	Andean structural control on interseismic coupling in the North Chile subduction zone. Nature Geoscience, 2013, 6, 462-467.	12.9	138
26	Coseismic and postseismic slip associated with the 2010 Maule Earthquake, Chile: Characterizing the Arauco Peninsula barrier effect. Journal of Geophysical Research: Solid Earth, 2013, 118, 3142-3159.	3.4	134
27	Interseismic crustal deformation in the Taiwan plate boundary zone revealed by GPS observations, seismicity, and earthquake focal mechanisms. Tectonophysics, 2009, 479, 4-18.	2.2	132
28	Accounting for prediction uncertainty when inferring subsurface fault slip. Geophysical Journal International, 2014, 197, 464-482.	2.4	128
29	Aseismic slip and seismogenic coupling along the central San Andreas Fault. Geophysical Research Letters, 2015, 42, 297-306.	4.0	123
30	Localization of the gravity field and the signature of glacial rebound. Nature, 1997, 390, 500-504.	27.8	121
31	Deformation and seismicity in the Coso geothermal area, Inyo County, California: Observations and modeling using satellite radar interferometry. Journal of Geophysical Research, 2000, 105, 21781-21793.	3.3	119
32	A multiscale approach to estimating topographically correlated propagation delays in radar interferograms. Geochemistry, Geophysics, Geosystems, 2010, 11, .	2.5	119
33	Co-seismic slip from the 1995 July 30Mw= 8.1 Antofagasta, Chile, earthquake as constrained by InSAR and GPS observations. Geophysical Journal International, 2002, 150, 362-376.	2.4	111
34	Multiscale InSAR Time Series (MInTS) analysis of surface deformation. Journal of Geophysical Research, 2012, 117, .	3.3	108
35	Rapid Damage Mapping for the 2015 <i>M</i> _w Â7.8 Gorkha Earthquake Using Synthetic Aperture Radar Data from COSMO–SkyMed and ALOS-2 Satellites. Seismological Research Letters, 2015, 86, 1549-1556.	1.9	108
36	An aseismic slip pulse in northern Chile and along-strike variations in seismogenic behavior. Journal of Geophysical Research, 2006, 111, .	3.3	107

#	Article	IF	CITATIONS
37	New Radar Interferometric Time Series Analysis Toolbox Released. Eos, 2013, 94, 69-70.	0.1	106
38	A two-dimensional dislocation model for interseismic deformation of the Taiwan mountain belt. Earth and Planetary Science Letters, 2003, 211, 287-294.	4.4	98
39	A noise model for InSAR time series. Journal of Geophysical Research: Solid Earth, 2015, 120, 2752-2771.	3.4	96
40	Preliminary Report on the 16 October 1999 M 7.1 Hector Mine, California, Earthquake. Seismological Research Letters, 2000, 71, 11-23.	1.9	91
41	The Iquique earthquake sequence of April 2014: Bayesian modeling accounting for prediction uncertainty. Geophysical Research Letters, 2015, 42, 7949-7957.	4.0	91
42	Source model of the 2007 <i>M</i> _{<i>w</i>} 8.0 Pisco, Peru earthquake: Implications for seismogenic behavior of subduction megathrusts. Journal of Geophysical Research, 2010, 115, .	3.3	88
43	Bayesian inversion for finite fault earthquake source models – II: the 2011 great Tohoku-oki, Japan earthquake. Geophysical Journal International, 2014, 198, 922-940.	2.4	86
44	InSAR Time-Series Estimation of the Ionospheric Phase Delay: An Extension of the Split Range-Spectrum Technique. IEEE Transactions on Geoscience and Remote Sensing, 2017, 55, 5984-5996.	6.3	81
45	Tidally induced variations in vertical and horizontal motion on Rutford Ice Stream, West Antarctica, inferred from remotely sensed observations. Journal of Geophysical Research F: Earth Surface, 2017, 122, 167-190.	2.8	80
46	Locations of selected small earthquakes in the Zagros mountains. Geochemistry, Geophysics, Geosystems, 2005, 6, n/a-n/a.	2.5	78
47	Finite source modelling of magmatic unrest in Socorro, NewÂMexico, and Long Valley, California. Geophysical Journal International, 2001, 146, 191-200.	2.4	77
48	The 2013 Mw 7.7 Balochistan Earthquake: Seismic Potential of an Accretionary Wedge. Bulletin of the Seismological Society of America, 2014, 104, 1020-1030.	2.3	77
49	An aseismic slip transient on the North Anatolian Fault. Geophysical Research Letters, 2016, 43, 3254-3262.	4.0	74
50	Asperities and barriers on the seismogenic zone in North Chile: state-of-the-art after the 2007 Mw 7.7 Tocopilla earthquake inferred by GPS and InSAR data. Geophysical Journal International, 2010, 183, 390-406.	2.4	73
51	Global Variations in the Geoid/Topography Admittance of Venus. Science, 1994, 264, 798-803.	12.6	70
52	Geodetic, teleseismic, and strong motion constraints on slip from recent southern Peru subduction zone earthquakes. Journal of Geophysical Research, 2007, 112, .	3.3	69
53	Post-seismic and interseismic fault creep II: transient creep and interseismic stress shadows on megathrusts. Geophysical Journal International, 2010, 181, 99-112.	2.4	69
54	Evidence for on-going inflation of the Socorro Magma Body, New Mexico, from interferometric synthetic aperture radar imaging. Geophysical Research Letters, 2001, 28, 3549-3552.	4.0	67

Mark Simons

#	Article	IF	CITATIONS
55	Fault-zone controls on the spatial distribution of slow-moving landslides. Bulletin of the Geological Society of America, 2013, 125, 473-489.	3.3	67
56	lonospheric Correction of InSAR Time Series Analysis of C-band Sentinel-1 TOPS Data. IEEE Transactions on Geoscience and Remote Sensing, 2019, 57, 6755-6773.	6.3	67
57	Accounting for uncertain fault geometry in earthquake source inversions – I: theory and simplified application. Geophysical Journal International, 2018, 214, 1174-1190.	2.4	65
58	Plains tectonism on Venus: The deformation belts of Lavinia Planitia. Journal of Geophysical Research, 1992, 97, 13579-13599.	3.3	64
59	Temporal clustering of major earthquakes along individual faults due to post-seismic reloading. Geophysical Journal International, 2004, 160, 179-194.	2.4	64
60	Interferometric Synthetic Aperture Radar Geodesy. , 2007, , 391-446.		64
61	Multiscale estimation of GPS velocity fields. Geophysical Journal International, 2009, 179, 945-971.	2.4	63
62	Processes controlling the downstream evolution of ice rheology in glacier shear margins: case study on Rutford Ice Stream, West Antarctica. Journal of Glaciology, 2018, 64, 583-594.	2.2	63
63	BARGEN continuous GPS data across the eastern Basin and Range province, and implications for fault system dynamics. Geophysical Journal International, 2004, 159, 842-862.	2.4	62
64	An InSAR-based survey of volcanic deformation in the southern Andes. Geophysical Research Letters, 2004, 31, .	4.0	60
65	Isolating alongâ€strike variations in the depth extent of shallow creep and fault locking on the northern Great Sumatran Fault. Journal of Geophysical Research, 2012, 117, .	3.3	60
66	Interferometric Synthetic Aperture Radar Geodesy. , 2007, , 391-446.		56
67	Location and mechanism of the Little Skull Mountain earthquake as constrained by satellite radar interferometry and seismic waveform modeling. Journal of Geophysical Research, 2002, 107, ETG 7-1.	3.3	54
68	Distribution of slip from 11Mw> 6 earthquakes in the northern Chile subduction zone. Journal of Geophysical Research, 2006, 111, .	3.3	54
69	A reappraisal of postglacial decay times from Richmond Gulf and James Bay, Canada. Geophysical Journal International, 2000, 142, 783-800.	2.4	53
70	The collapse of Bárðarbunga caldera, Iceland. Geophysical Journal International, 2015, 202, 446-453.	2.4	51
71	On the Synergistic Use of SAR Constellations' Data Exploitation for Earth Science and Natural Hazard Response. IEEE Journal of Selected Topics in Applied Earth Observations and Remote Sensing, 2016, 9, 1095-1100.	4.9	47
72	Plastic bed beneath Hofsjökull Ice Cap, central Iceland, and the sensitivity of ice flow to surface meltwater flux. Journal of Glaciology, 2016, 62, 147-158.	2.2	46

#	Article	IF	CITATIONS
73	Quantifying Ground Deformation in the Los Angeles and Santa Ana Coastal Basins Due to Groundwater Withdrawal. Water Resources Research, 2018, 54, 3557-3582.	4.2	46
74	Three-dimensional FEM derived elastic Green's functions for the coseismic deformation of the 2005 <i>M</i> _{<i>w</i>} 8.7 Nias-Simeulue, Sumatra earthquake. Geochemistry, Geophysics, Geosystems, 2011, 12, n/a-n/a.	2.5	42
75	Surveying Volcanic Arcs with Satellite Radar Interferometry: The Central Andes, Kamchatka, and Beyond. GSA Today, 2004, 14, 4.	2.0	41
76	Probing Asthenospheric Density, Temperature, and Elastic Moduli Below the Western United States. Science, 2011, 332, 947-951.	12.6	41
77	The potential for a great earthquake along the southernmost Ryukyu subduction zone. Geophysical Research Letters, 2012, 39, .	4.0	41
78	Depth varying rupture properties during the 2015 Mw 7.8 Gorkha (Nepal) earthquake. Tectonophysics, 2017, 714-715, 44-54.	2.2	40
79	The Chilean GNSS Network: Current Status and Progress toward Early Warning Applications. Seismological Research Letters, 2018, 89, 1546-1554.	1.9	40
80	Anomalously steep dips of earthquakes in the 2011 Tohoku-Oki source region and possible explanations. Earth and Planetary Science Letters, 2012, 353-354, 121-133.	4.4	39
81	Detecting transient signals in geodetic time series using sparse estimation techniques. Journal of Geophysical Research: Solid Earth, 2014, 119, 5140-5160.	3.4	37
82	Observations of ocean tidal load response in South America from subdaily GPS positions. Geophysical Journal International, 2016, 205, 1637-1664.	2.4	37
83	Surface Deformation Related to the 2019 MwÂ7.1 and 6.4 Ridgecrest Earthquakes in California from GPS, SAR Interferometry, and SAR Pixel Offsets. Seismological Research Letters, 2020, 91, 2035-2046.	1.9	37
84	Importance of ocean tidal load corrections for differential InSAR. Geophysical Research Letters, 2008, 35, .	4.0	36
85	Post-seismic reloading and temporal clustering on a single fault. Geophysical Journal International, 2008, 172, 581-592.	2.4	33
86	Interseismic Loading of Subduction Megathrust Drives Longâ€Term Uplift in Northern Chile. Geophysical Research Letters, 2020, 47, e2019GL085377.	4.0	33
87	An elastic plate model for interseismic deformation in subduction zones. Journal of Geophysical Research, 2010, 115, .	3.3	31
88	LoadDef: A Pythonâ€Based Toolkit to Model Elastic Deformation Caused by Surface Mass Loading on Spherically Symmetric Bodies. Earth and Space Science, 2019, 6, 311-323.	2.6	30
89	Interferometric Synthetic Aperture Radar Geodesy. , 2015, , 339-385.		29
90	Post-seismic and interseismic fault creep I: model description. Geophysical Journal International, 2010, 181, 81-98.	2.4	28

Mark Simons

#	Article	IF	CITATIONS
91	A Bayesian source model for the 2004 great Sumatraâ€Andaman earthquake. Journal of Geophysical Research: Solid Earth, 2016, 121, 5116-5135.	3.4	28
92	Modeling the elastic transmission of tidal stresses to great distances inland in channelized ice streams. Cryosphere, 2014, 8, 2007-2029.	3.9	27
93	The 2010 <i>M</i> _w 8.8 Maule, Chile earthquake: Nucleation and rupture propagation controlled by a subducted topographic high. Geophysical Research Letters, 2012, 39, .	4.0	26
94	Revisiting the 1992 Landers earthquake: a Bayesian exploration of co-seismic slip and off-fault damage. Geophysical Journal International, 2018, 212, 839-852.	2.4	26
95	Tidal modulation of ice shelf buttressing stresses. Annals of Glaciology, 2017, 58, 12-20.	1.4	25
96	Shallow Rupture of the 2011 Tarlay Earthquake (Mw 6.8), Eastern Myanmar. Bulletin of the Seismological Society of America, 2014, 104, 2904-2914.	2.3	24
97	High interseismic coupling in the Eastern Makran (Pakistan) subduction zone. Earth and Planetary Science Letters, 2015, 420, 116-126.	4.4	24
98	The sensitivity of surface mass loading displacement response to perturbations in the elastic structure of the crust and mantle. Journal of Geophysical Research: Solid Earth, 2016, 121, 3911-3938.	3.4	24
99	The InSAR Scientific Computing Environment 3.0: A Flexible Framework for NISAR Operational and User-Led Science Processing. , 2018, , .		23
100	The Information Content of Pore Fluid δ18O and [Clâ^']. Journal of Physical Oceanography, 2015, 45, 2070-2094.	1.7	22
101	Strain budget of the Ecuador–Colombia subduction zone: A stochastic view. Earth and Planetary Science Letters, 2018, 498, 288-299.	4.4	22
102	Estimates of aseismic slip associated with small earthquakes near San Juan Bautista, CA. Journal of Geophysical Research: Solid Earth, 2016, 121, 8254-8275.	3.4	21
103	Accounting for uncertain fault geometry in earthquake source inversions – II: application to the Mw 6.2 Amatrice earthquake, central Italy. Geophysical Journal International, 2019, 218, 689-707.	2.4	21
104	Estimation of interplate coupling in the Nankai trough, Japan using GPS data from 1996 to 2006. Geophysical Journal International, 2010, , .	2.4	20
105	Early melt season velocity fields of Langjökull and Hofsjökull, central Iceland. Journal of Glaciology, 2015, 61, 253-266.	2.2	20
106	A survey of volcanic deformation on Java using ALOS PALSAR interferometric time series. Geochemistry, Geophysics, Geosystems, 2011, 12, n/a-n/a.	2.5	19
107	Range Geolocation Accuracy of C-/L-Band SAR and its Implications for Operational Stack Coregistration. IEEE Transactions on Geoscience and Remote Sensing, 2022, 60, 1-19.	6.3	18
108	On Closure Phase and Systematic Bias in Multilooked SAR Interferometry. IEEE Transactions on Geoscience and Remote Sensing, 2022, 60, 1-11.	6.3	15

#	Article	IF	CITATIONS
109	Integration of transient strain events with models of plate coupling and areas of great earthquakes in southwest Japan. Geophysical Journal International, 2010, , .	2.4	14
110	Introduction to the Special Issue on the 2011 Tohoku Earthquake and Tsunami. Bulletin of the Seismological Society of America, 2013, 103, 1165-1170.	2.3	14
111	Deep Learning-Based Damage Mapping With InSAR Coherence Time Series. IEEE Transactions on Geoscience and Remote Sensing, 2022, 60, 1-17.	6.3	13
112	Observation of Core Phase ScS from the Mw 9.0 Tohoku-Oki Earthquake with High-Rate GPS. Seismological Research Letters, 2013, 84, 594-599.	1.9	12
113	A Stochastic View of the 2020 Elazığ M w 6.8 Earthquake (Turkey). Geophysical Research Letters, 2021, 48, e2020GL090704.	4.0	12
114	Practical implications of the geometrical sensitivity of elastic dislocation models for field geologic surveys. Tectonophysics, 2012, 560-561, 94-104.	2.2	11
115	Probabilistic imaging of tsunamigenic seafloor deformation during the 2011 Tohokuâ€oki Earthquake. Journal of Geophysical Research: Solid Earth, 2016, 121, 9050-9076.	3.4	11
116	Geodetic Imaging of Time-Dependent Three-Component Surface Deformation: Application to Tidal-Timescale Ice Flow of Rutford Ice Stream, West Antarctica. IEEE Transactions on Geoscience and Remote Sensing, 2017, 55, 5515-5524.	6.3	11
117	An EPIC Tikhonov Regularization: Application to Quasi tatic Fault Slip Inversion. Journal of Geophysical Research: Solid Earth, 2021, 126, e2020JB021141.	3.4	10
118	An asperity model for fault creep and interseismic deformation in northeastern Japan. Geophysical Journal International, 2013, 192, 38-57.	2.4	9
119	Rapid Imaging of Earthquake Ruptures with Combined Geodetic and Seismic Analysis. Procedia Technology, 2014, 16, 876-885.	1.1	9
120	A comparison of predicted and observed ocean tidal loading in Alaska. Geophysical Journal International, 2020, 223, 454-470.	2.4	9
121	Accounting for uncertain 3-D elastic structure in fault slip estimates. Geophysical Journal International, 2020, 224, 1404-1421.	2.4	8
122	Plan for living on a restless planet sets NASA's solid Earth agenda. Eos, 2003, 84, 485.	0.1	7
123	A Multipixel Time Series Analysis Method Accounting for Ground Motion, Atmospheric Noise, and Orbital Errors. Geophysical Research Letters, 2018, 45, 1814-1824.	4.0	7
124	A Method for Calibration of the Local Magnitude Scale Based on Relative Spectral Amplitudes, and Application to the San Juan Bautista, California, Area. Bulletin of the Seismological Society of America, 2017, 107, 85-96.	2.3	6
125	Multiple glacier surges observed with airborne and spaceborne interferometric synthetic aperture radar. , 2015, , .		2
126	Using InSAR Time Series to Monitor Surface Fractures and Fissures in the Al-Yutamah Valley, Western Arabia. Remote Sensing, 2022, 14, 1769.	4.0	2

8

#	Article	IF	CITATIONS
127	Recent rapid disaster response products derived from COSMO-Skymed synthetic aperture radar data. , 2016, , .		0
128	3D velocity field time series using synthetic aperture radar: application to tidal-timescale ice-flow variability in Rutford Ice Stream, West Antarctica. Proceedings of SPIE, 2016, , .	0.8	0
129	Imaging Complex Fault Slip of Large Earthquakes with Sentinel-1 and ALOS-2 SAR Analysis and Other Geodetic and Seismic Data. , 2021, , .		0